Available online at www.sciencedirect.com

ScienceDirect

IFAC PapersOnLine 52-5 (2019) 134–140

Minimum-fuel Engine On/Off Control for the Energy Management of a Hybrid Electric Vehicle via Iterative Linear Programming ⋆

Nicolò Robuschi * **Mauro Salazar** ** **Pol Duhr** **
Francesco Braghin * **Christopher H. Onder** **

* *Department of Mechanical Engineering, Politecnico di Milano, 20156 Milano, Italy* ({nicolo.robuschi,francesco.braghin}@polimi.it)
** *Institute for Dynamic Systems and Control, ETH Zürich, 8092 Zürich, Switzerland* ({maurosalazar,pduhr}@idsc.mavt.ethz.ch)

The first two authors contributed equally to this paper.

Abstract: In this paper we present models and optimization algorithms to rapidly compute the fuel-optimal energy management strategies of a hybrid electric powertrain for a given driving cycle. Specifically, we first identify a mixed-integer model of the system, including the engine on/off signal. Thereafter, by carefully relaxing the fuel-optimal control problem to a linear program, we devise an iterative algorithm to rapidly compute the minimum-fuel energy management strategies. We validate our approach by comparing its solution with the globally optimal one obtained solving the mixed-integer linear problem and demonstrate its effectiveness by assessing the impact of different battery charge targets on the achievable fuel consumption. Numerical results show that the proposed algorithm can assess fuel-optimal control strategies in a few seconds, paving the way for extensive parameter studies and real-time implementations.

Keywords: Hybrid vehicles, energy management, supervisory control, mixed-integer optimal control, convex optimization, linear programming.

1. INTRODUCTION

In order to reduce fuel consumption and pollutant emissions, the automotive sector has been introducing hybrid electric powertrains for passenger cars and trucks. The topology of the propulsion system and the components' sizing have a significant impact on the achievable performance, as well as the energy management algorithms coordinating the powertrain components [Guzzella and Sciarretta, 2013].

In this paper, we will focus on the powertrain shown in Fig. 1, consisting of an internal combustion engine and an electric motor (EM) providing boosting and regenerative braking. The engine is connected to an automated gearbox, while the electric motor is coupled to the output shaft of that gearbox with an additional gear set. The final drive and the differential (FD) transmit the propulsive power to the wheels. The fuel tank and the battery are the on-board energy storages.

There exist several contributions on the synthesis of high-level energy management strategies for hybrid electric vehicles (HEVs). In particular, causal feedback control schemes are mostly based on ECMS [Nüesch et al., 2014a; Salazar et al., 2018], rule-based strategies [Hofman et al., 2007] or MPC [Johannesson et al., 2015; Salazar et al., 2017a], whilst non-causal control strategies have been computed using convex optimization [Nüesch et al., 2014b; Ebbesen et al., 2018], Pontryagin's minimum principle [Guzzella and Sciarretta, 2013; Salazar et al., 2017b] and dynamic programming [Elbert et al., 2013]. The latter approaches assess the optimal fuel consumption over a given driving cycle and can therefore be used to benchmark causal controllers or investigate the impact of different powertrain structures on the achievable performance. While delivering very satisfying results, such methodologies rely on optimization algorithms resulting in computational times in the order of minutes to hours.

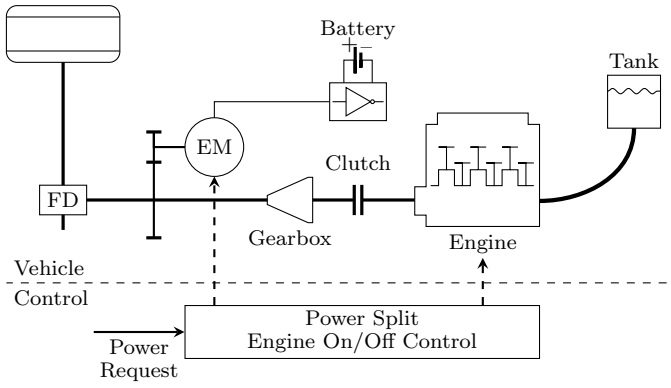

Fig. 1. Hybrid electric powertrain with the energy management system.

This paper presents a non-causal approach to rapidly compute the fuel-optimal control strategies of a hybrid electric powertrain for a given driving cycle, including the engine on/off signal. We use an iterative algorithm that enables us to assess the minimum-fuel operation in a few seconds, allowing for extensive parameter studies to be performed rapidly.

The structure of this paper is as follows: Section 2 presents a piecewise affine model of the HEV shown in Fig. 1 and formulates the minimum-fuel control problem as a mixed-

⋆ We thank Ferrari S.p.A. for supporting this project.

10.1016/j.ifacol.2019.09.022

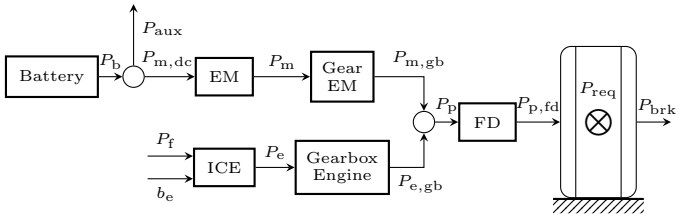

Fig. 2. Schematic representation with the power flows of the powertrain.

integer linear program (MILP). In Section 3, we present sequential and bisection algorithms to rapidly solve the fuel-optimal control problem as a sequence of linear programs (LP) iterating on the engine on/off variable. Section 4 compares the results obtained with our approach to the globally optimal solution of the MILP for a standard driving cycle and presents a parameter study on the impact of the battery targets on the achievable fuel consumption. Section 5 concludes the paper and provides future research directions.

2. MODEL AND OPTIMAL CONTROL PROBLEM

In this section, we first identify a piecewise affine model of the HEV and then formulate the fuel-optimal control problem. Finally, we discretize the model and parse it as a MILP. For reasons of confidentiality, all sensitive data shown throughout this paper have been normalized.

2.1 Powertrain Model

We model the powertrain schematically drawn in Fig. 2 in the time domain and assume that the velocity and the gearshift profiles of the driving cycle are known. Therefore, the power request $P_{\mathrm{req}}(t)$ that has to be delivered at the wheels as well as the engine and motor speeds $\omega_{\mathrm{e}}(t), \omega_{\mathrm{m}}(t)$, respectively, are exogenous variables. In the following modeling equations, we drop the time dependency to ease the notation.

The engine power P_{e} can be captured by a speed-dependent Willans approximation [Guzzella and Onder, 2010] as a function of the fuel power $P_{\mathrm{f}} \geq 0$, the engine efficiency $e(\omega_{\mathrm{e}})$ and the drag power $P_{\mathrm{e},0}(\omega_{\mathrm{e}})$ as

$$P_{\mathrm{e}} = \big(e(\omega_{\mathrm{e}}) \cdot P_{\mathrm{f}} - P_{\mathrm{e},0}(\omega_{\mathrm{e}})\big) \cdot b_{\mathrm{e}} \ , \tag{1}$$

where $b_{\mathrm{e}} \in \{0,1\}$ is the engine on/off decision variable (0 corresponding to off, 1 to on). Thereby we assume the clutch between the engine and the gearbox to be open whenever the engine is off. Fig. 3 shows that this model is in good agreement with the measurement data. The maximum engine power is speed-dependent, i.e.,

$$P_{\mathrm{e}} \leq P_{\mathrm{e,max}}(\omega_{\mathrm{e}}) \ . \tag{2}$$

Since Eq. (1) is non-convex, we rewrite it using the so-called big-M formulation [Richards and How, 2005] as

$$\begin{aligned} P_{\mathrm{e}} &\leq e(\omega_{\mathrm{e}}) \cdot P_{\mathrm{f}} - P_{\mathrm{e},0}(\omega_{\mathrm{e}}) + (1 - b_{\mathrm{e}}) \cdot M \\ P_{\mathrm{e}} &\geq e(\omega_{\mathrm{e}}) \cdot P_{\mathrm{f}} - P_{\mathrm{e},0}(\omega_{\mathrm{e}}) - (1 - b_{\mathrm{e}}) \cdot M \\ P_{\mathrm{e}} &\leq b_{\mathrm{e}} \cdot M \\ P_{\mathrm{e}} &\geq -b_{\mathrm{e}} \cdot M \ , \end{aligned} \tag{3}$$

where $M \geq \sup_{P_{\mathrm{e}}} |P_{\mathrm{e}}|$. The engine power transmitted through the gearbox $P_{\mathrm{e,gb}}$ is then modeled using the gearbox efficiency $\eta_{\mathrm{gb,e}}$ as

$$P_{\mathrm{e,gb}} = \begin{cases} \dfrac{1}{\eta_{\mathrm{gb,e}}} \cdot P_{\mathrm{e}} & \text{if } P_{\mathrm{e}} < 0 \\ \eta_{\mathrm{gb,e}} \cdot P_{\mathrm{e}} & \text{if } P_{\mathrm{e}} \geq 0 \ . \end{cases} \tag{4}$$

Since $0 < \eta_{\mathrm{gb,e}} \leq 1$ holds, we can relax Eq. (4) to a set of convex inequality constraints as

$$\begin{aligned} P_{\mathrm{e,gb}} &\leq \frac{1}{\eta_{\mathrm{gb,e}}} \cdot P_{\mathrm{e}} \\ P_{\mathrm{e,gb}} &\leq \eta_{\mathrm{gb,e}} \cdot P_{\mathrm{e}} \ . \end{aligned} \tag{5}$$

If the optimization criterion is chosen to minimize the energy consumption, then the constraints (5) will be active, holding with equality [Murgovski et al., 2015]. In the following, we will apply this relaxation technique to several other modeling equations. For the electric drive, the conversion losses from electrical to mechanical power and vice-versa are modeled by the piecewise affine relation

$$P_{\mathrm{m,dc}} = \begin{cases} \eta_{\mathrm{m}}^{\mathrm{g}}(\omega_{\mathrm{m}}) \cdot P_{\mathrm{m}} & \text{if } P_{\mathrm{m}} < 0 \\ \dfrac{1}{\eta_{\mathrm{m}}^{\mathrm{m}}(\omega_{\mathrm{m}})} \cdot P_{\mathrm{m}} & \text{if } P_{\mathrm{m}} \geq 0 \ , \end{cases} \tag{6}$$

with $P_{\mathrm{m,dc}}$ and P_{m} representing the electrical and mechanical motor power, respectively, whilst the speed-dependent efficiencies $\eta_{\mathrm{m}}^{\mathrm{m}}$ and $\eta_{\mathrm{m}}^{\mathrm{g}}$ (in motor and generator mode, respectively) are subject to identification. Fig. 3 shows a comparison of measurement data with the model identified. Since $\eta_{\mathrm{m}}^{\mathrm{g}}(\omega_{\mathrm{m}}), \eta_{\mathrm{m}}^{\mathrm{m}}(\omega_{\mathrm{m}}) \in (0,1]$ holds for all ω_{m}, we also relax Eq. (6) to a set of linear inequality constraints:

$$\begin{aligned} P_{\mathrm{m,dc}} &\geq \eta_{\mathrm{m}}^{\mathrm{g}}(\omega_{\mathrm{m}}) \cdot P_{\mathrm{m}} \\ P_{\mathrm{m,dc}} &\geq \frac{1}{\eta_{\mathrm{m}}^{\mathrm{m}}(\omega_{\mathrm{m}})} \cdot P_{\mathrm{m}} \ . \end{aligned} \tag{7}$$

The operating bounds of the electric motor are also speed-dependent, i.e.,

$$P_{\mathrm{m,min}}(\omega_{\mathrm{m}}) \leq P_{\mathrm{m}} \leq P_{\mathrm{m,max}}(\omega_{\mathrm{m}}) \ . \tag{8}$$

By introducing the efficiency $\eta_{\mathrm{gb,m}}$, the mechanical power $P_{\mathrm{m,gb}}$ transmitted by the motor through the gear set is given by

$$P_{\mathrm{m,gb}} = \begin{cases} \dfrac{1}{\eta_{\mathrm{gb,m}}} \cdot P_{\mathrm{m}} & \text{if } P_{\mathrm{m}} < 0 \\ \eta_{\mathrm{gb,m}} \cdot P_{\mathrm{m}} & \text{if } P_{\mathrm{m}} \geq 0 \ . \end{cases} \tag{9}$$

Again, $0 < \eta_{\mathrm{gb,m}} \leq 1$ holds, and therefore we can also relax Eq. (9) to inequality as

$$\begin{aligned} P_{\mathrm{m,gb}} &\leq \frac{1}{\eta_{\mathrm{gb,m}}} \cdot P_{\mathrm{m}} \\ P_{\mathrm{m,gb}} &\leq \eta_{\mathrm{gb,m}} \cdot P_{\mathrm{m}} \ . \end{aligned} \tag{10}$$

The power at the terminals of the battery is given by

$$P_{\mathrm{b}} = P_{\mathrm{m,dc}} + P_{\mathrm{aux}} \ , \tag{11}$$

where P_{aux} models a constant auxiliary power flow. Introducing the loss coefficients $\eta_{\mathrm{b}}^{\mathrm{c}}$ and $\eta_{\mathrm{b}}^{\mathrm{d}}$ for charging and discharging, respectively, and assuming a constant open circuit voltage, the internal battery power P_{i} is modeled by the piecewise affine relation

$$P_{\mathrm{i}} = \begin{cases} \eta_{\mathrm{b}}^{\mathrm{c}} \cdot P_{\mathrm{b}} & \text{if } P_{\mathrm{b}} < 0 \\ \dfrac{1}{\eta_{\mathrm{b}}^{\mathrm{d}}} \cdot P_{\mathrm{b}} & \text{if } P_{\mathrm{b}} \geq 0 \ . \end{cases} \tag{12}$$

The results of the fit are shown in Fig. 4, together with the root mean square error. Because $\frac{1}{\eta_{\mathrm{b}}^{\mathrm{d}}} \geq \eta_{\mathrm{b}}^{\mathrm{c}}$ holds, we also relax Eq. (12) to a set of linear inequality constraints:

$$\begin{aligned} P_{\mathrm{i}} &\geq \eta_{\mathrm{b}}^{\mathrm{c}} \cdot P_{\mathrm{b}} \\ P_{\mathrm{i}} &\geq \frac{1}{\eta_{\mathrm{b}}^{\mathrm{d}}} \cdot P_{\mathrm{b}} \ . \end{aligned} \tag{13}$$

The total power delivered by the powertrain through the gearbox is given by

$$P_{\mathrm{p}} = P_{\mathrm{m,gb}} + P_{\mathrm{e,gb}} \ . \tag{14}$$

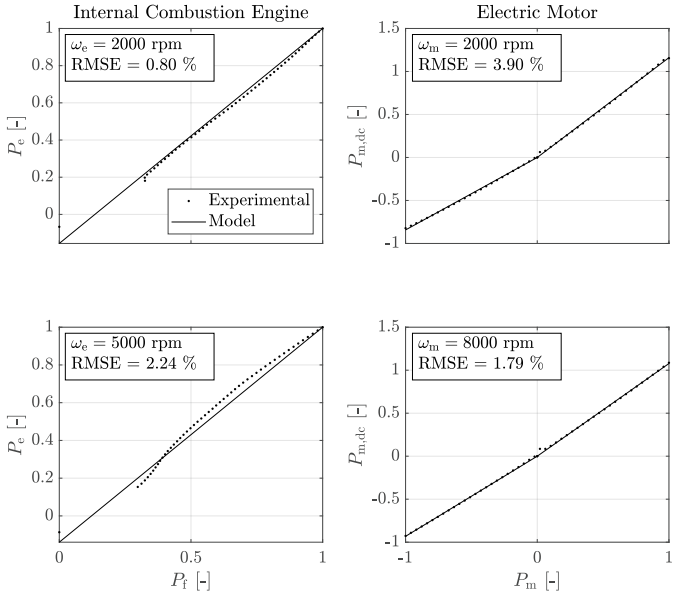

Fig. 3. Comparison of the piecewise affine models for the engine and the electric motor with measurement data for two different speed levels.

We model the losses in the differential and the final drive by introducing the efficiency η_{fd} as

$$P_{\mathrm{p,fd}} = \begin{cases} \dfrac{1}{\eta_{\mathrm{fd}}} \cdot P_{\mathrm{p}} & \text{if } P_{\mathrm{p}} < 0 \\ \eta_{\mathrm{fd}} \cdot P_{\mathrm{p}} & \text{if } P_{\mathrm{p}} \geq 0 \ . \end{cases} \tag{15}$$

Since we have $\eta_{\mathrm{fd}} \leq 1$, we can again relax to the following set of inequality constraints:

$$\begin{aligned} P_{\mathrm{p,fd}} &\leq \frac{1}{\eta_{\mathrm{fd}}} \cdot P_{\mathrm{p}} \\ P_{\mathrm{p,fd}} &\leq \eta_{\mathrm{fd}} \cdot P_{\mathrm{p}} \ . \end{aligned} \tag{16}$$

Finally, the exogenous power request has to be fulfilled by satisfying the equality constraint

$$P_{\mathrm{req}} = P_{\mathrm{p,fd}} - P_{\mathrm{brk}} \ , \tag{17}$$

where $P_{\mathrm{brk}} \geq 0$ is the power dissipated in the hydraulic brakes. Since we are not interested in the braking strategy, we can reformulate Eq. (17) as

$$P_{\mathrm{req}} \leq P_{\mathrm{p,fd}} \ . \tag{18}$$

The only state variable of the powertrain is the battery energy, which we model as an open integrator

$$\frac{\mathrm{d}}{\mathrm{d}t} E_{\mathrm{b}}(t) = -P_{\mathrm{i}}(t) \ , \tag{19}$$

where the minus sign is due to the fact that the battery is discharged when $P_{\mathrm{i}} > 0$. Finally, E_{b} must fulfill the following path constraint:

$$E_{\mathrm{b,min}} \leq E_{\mathrm{b}} \leq E_{\mathrm{b,max}} \ . \tag{20}$$

2.2 Fuel-optimal Control Problem

We formulate the minimum-fuel control problem to assess the optimal power-split and engine on/off strategies as follows:

$$\begin{aligned} &\min \int_0^T P_{\mathrm{f}} \, \mathrm{d}t \\ &\text{s.t. } (2), (3), (5), (7), (8), (10), (11), \\ &\quad (13), (14), (16), (18), (19), (20) \\ &\quad E_{\mathrm{b}}(0) = E_{\mathrm{b,0}} \\ &\quad E_{\mathrm{b}}(T) = E_{\mathrm{b,target}} \ , \end{aligned} \tag{21}$$

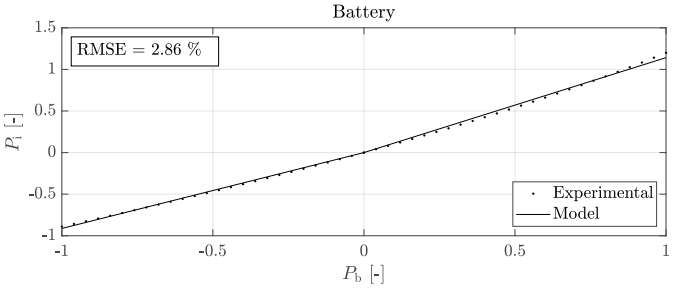

Fig. 4. Piecewise affine model of the battery and comparison to measurement data.

where $E_{\mathrm{b,0}}$ and $E_{\mathrm{b,target}}$ are the initial and targeted final battery states of energy, respectively.

2.3 Mixed-integer Linear Program Formulation

We discretize the powertrain model formulated above using the explicit Euler scheme with a sampling time T_{s} and a time horizon T. The derivative of a continuous-time variable $x(t)$ is thus approximated as

$$\frac{\mathrm{d}x}{\mathrm{d}t}(t) \approx \frac{x(t + T_{\mathrm{s}}) - x(t)}{T_{\mathrm{s}}} \ . \tag{22}$$

Let $N := \mathrm{ceil}(T/T_{\mathrm{s}})$ be the discrete-time horizon. Furthermore, we define $x[k] := x(k\,T_{\mathrm{s}})$, where $k \in \{0, \ldots, N\}$. We assume that the exogenous signals $\omega_{\mathrm{e}}[k]$, $\omega_{\mathrm{m}}[k]$ and $P_{\mathrm{req}}[k]$ are known for all $k \in \{0, \ldots, N-1\}$.

The state variable is $x = E_{\mathrm{b}} \in \mathbb{R}^N$, and the input variables are $u = \big(P_{\mathrm{m}}, b_{\mathrm{e}}\big) \in \mathbb{R}^{N-1} \times \{0,1\}^{N-1}$. The resulting fuel-optimal optimization problem (21) becomes

$$\min \sum_{k=0}^{N-1} P_{\mathrm{f}}[k] \cdot T_{\mathrm{s}} \ , \tag{23}$$

subject to the dynamics

$$E_{\mathrm{b}}[k+1] = E_{\mathrm{b}}[k] - P_{\mathrm{i}}[k] \cdot T_{\mathrm{s}} \ , \tag{24}$$

the state constraints on the battery state-of-charge

$$\begin{aligned} E_{\mathrm{b}}[0] &= E_{\mathrm{b,0}} \\ E_{\mathrm{b}}[N] &= E_{\mathrm{b,target}} \\ E_{\mathrm{b,min}} &\leq E_{\mathrm{b}}[k] \leq E_{\mathrm{b,max}} \ , \end{aligned} \tag{25}$$

the input constraints

$$\begin{aligned} b_{\mathrm{e}}[k] &\in \{0,1\} \\ P_{\mathrm{m}}[k] &\in \big[P_{\mathrm{m,min}}(\omega_{\mathrm{m}}[k]), P_{\mathrm{m,max}}(\omega_{\mathrm{m}}[k])\big] \ , \end{aligned} \tag{26}$$

the system equality constraints

$$P_{\mathrm{p}}[k] = P_{\mathrm{m,gb}}[k] + P_{\mathrm{e,gb}}[k], \tag{27}$$

the system inequality constraints

$$
\begin{aligned}
P_{\mathrm{f}}[k] &\geq 0 \\
P_{\mathrm{e}}[k] &\leq P_{\mathrm{e,max}}(\omega_{\mathrm{e}}[k]) \\
P_{\mathrm{e,gb}}[k] &\leq \frac{1}{\eta_{\mathrm{gb,e}}} \cdot P_{\mathrm{e}}[k] \\
P_{\mathrm{e,gb}}[k] &\leq \eta_{\mathrm{gb,e}} \cdot P_{\mathrm{e}}[k] \\
P_{\mathrm{m,dc}}[k] &\geq \eta_{\mathrm{m}}^{\mathrm{g}}(\omega_{\mathrm{m}}[k]) \cdot P_{\mathrm{m}}[k] \\
P_{\mathrm{m,dc}}[k] &\geq \frac{1}{\eta_{\mathrm{m}}^{\mathrm{m}}(\omega_{\mathrm{m}}[k])} \cdot P_{\mathrm{m}}[k] \\
P_{\mathrm{m}}[k] &\geq \eta_{\mathrm{gb,m}} \cdot P_{\mathrm{m,gb}}[k] \\
P_{\mathrm{m}}[k] &\geq \frac{1}{\eta_{\mathrm{gb,m}}} \cdot P_{\mathrm{m,gb}}[k] \\
P_{\mathrm{i}}[k] &\geq \eta_{\mathrm{b}}^{\mathrm{c}} \cdot P_{\mathrm{b}}[k] \\
P_{\mathrm{i}}[k] &\geq \frac{1}{\eta_{\mathrm{b}}^{\mathrm{d}}} \cdot P_{\mathrm{b}}[k] \\
P_{\mathrm{p,fd}}[k] &\leq \frac{1}{\eta_{\mathrm{fd}}} \cdot P_{\mathrm{p}}[k] \\
P_{\mathrm{p,fd}}[k] &\leq \eta_{\mathrm{fd}} \cdot P_{\mathrm{p}}[k] \\
P_{\mathrm{p,fd}}[k] &\geq P_{\mathrm{req}}[k] \ ,
\end{aligned}
\tag{28}
$$

and the system inequality constraints with binary variables

$$
\begin{aligned}
&P_{\mathrm{e}}[k] \geq e(\omega_{\mathrm{e}}[k]) \cdot P_{\mathrm{f}}[k] - P_{\mathrm{e},0}(\omega_{\mathrm{e}}[k]) - (1 - b_{\mathrm{e}}[k]) \cdot M \\
&P_{\mathrm{e}}[k] \leq e(\omega_{\mathrm{e}}[k]) \cdot P_{\mathrm{f}}[k] - P_{\mathrm{e},0}(\omega_{\mathrm{e}}[k]) + (1 - b_{\mathrm{e}}[k]) \cdot M \\
&P_{\mathrm{e}}[k] \geq -b_{\mathrm{e}}[k] \cdot M \\
&P_{\mathrm{e}}[k] \leq b_{\mathrm{e}}[k] \cdot M \ .
\end{aligned}
\tag{29}
$$

3. ALGORITHM

This section presents a threshold-based linear programming (TB-LP) algorithm to solve the minimum-fuel engine on/off and power split control problem presented in Section 2.2. The main goal is to rapidly solve the MILP presented in Section 2.3 in an iterative fashion. Fig. 5 shows a schematic representation of the algorithm, highlighting an inner and an outer loop. Iterating on the engine on/off signal b_{e}, the inner branch solves Problem (21) as a two-point boundary value problem (TPBVP), whereby the initial and final battery state of charge are given whilst the path constraints on the battery energy are ignored. The outer branch is a multi-point boundary value problem (MPBVP) solver built upon [Rousseau et al., 2007] checking whether the battery path constraints are respected by the solution of the TPBVP solved by the inner loop. If this is not the case, the solver splits up the problem into subproblems that are fed to the inner loop as TPBVPs. In this paper we solely focus on scenarios where the lower battery state constraint $E_{\mathrm{b,min}}$ may become active over the cycle, since this is the most common case in standard driving cycles. Such an approach is readily extendable to introduce also the upper path constraint. The proposed algorithm consists of the three steps delineated in the following three subsections.

3.1 MILP Relaxed to LP

We perform a convex relaxation on the Willans approximation of the engine (1). As a result we obtain the gray convex hull shown in Fig. 6. Since the minimum-fuel control strategy would then always operate the engine on the maximum efficiency dash-dotted line of Fig. 6, we can reformulate Eq. (1) by substituting P_{f} with the maximum fuel power that the engine can deliver $P_{\mathrm{f,max}}$ and relaxing the binary on/off variable as $b_{\mathrm{e}}^{\mathrm{rlx}} \in [0, 1]$. The engine power P_{e} is therefore

$$
P_{\mathrm{e}} = (e(\omega_{\mathrm{e}}) \cdot P_{\mathrm{f,max}}(\omega_{\mathrm{e}}) - P_{\mathrm{e},0}(\omega_{\mathrm{e}})) \cdot b_{\mathrm{e}}^{\mathrm{rlx}} \ , \tag{30}
$$

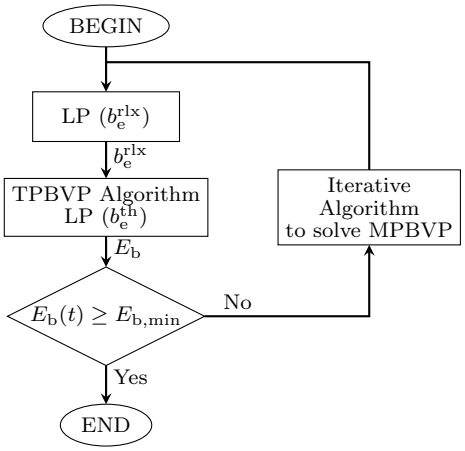

Fig. 5. The proposed TB-LP algorithm.

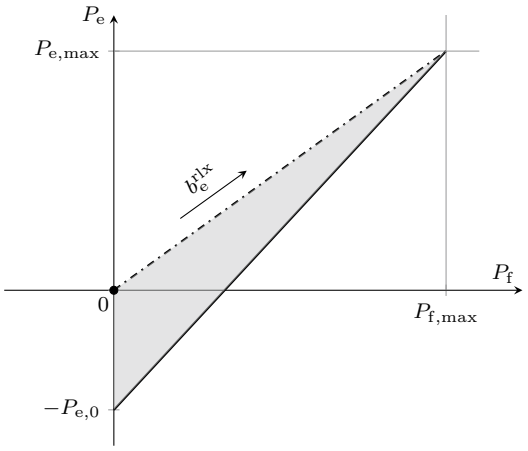

Fig. 6. Willans approximation and relaxation at a given engine speed.

where the maximum fuel power $P_{\mathrm{f,max}}$ at every time instant is defined by the relationship

$$
P_{\mathrm{f,max}}(\omega_{\mathrm{e}}) = \frac{P_{\mathrm{e,max}}(\omega_{\mathrm{e}}) + P_{\mathrm{e},0}(\omega_{\mathrm{e}})}{e(\omega_{\mathrm{e}})} \ . \tag{31}
$$

This way, we cast the problem into a linear form and we allow the engine to operate over the dash-dotted line depicted in Fig. 6. The engine operating points can span between maximum engine power when $b_{\mathrm{e}}^{\mathrm{rlx}}$ equals one and turned-off condition when $b_{\mathrm{e}}^{\mathrm{rlx}}$ equals zero.

The engine power P_{e} is therefore found solving a linear program where the optimization variables are the mechanical power provided by the electric motor P_{m} and the continuous variable $b_{\mathrm{e}}^{\mathrm{rlx}}$ regulating the power delivered by the engine. Since the operating points of the engine can span over the dash-dotted line corresponding to the most efficient engine operating zone, this yields a lower bound on the achievable fuel consumption. Specifically, the relaxed problem is

$$
\begin{aligned}
&\min \int_0^T P_{\mathrm{f}} \, \mathrm{d}t \\
&\text{s.t. } (5), (7), (8), (10), (11), (13), \\
&\quad (14), (16), (18), (19), (20), (30), (31) \\
&\quad b_{\mathrm{e}}^{\mathrm{rlx}}(t) \in [0, 1] \\
&\quad E_{\mathrm{b}}(0) = E_{\mathrm{b},0} \\
&\quad E_{\mathrm{b}}(T) = E_{\mathrm{b,target}} \ .
\end{aligned}
\tag{32}
$$

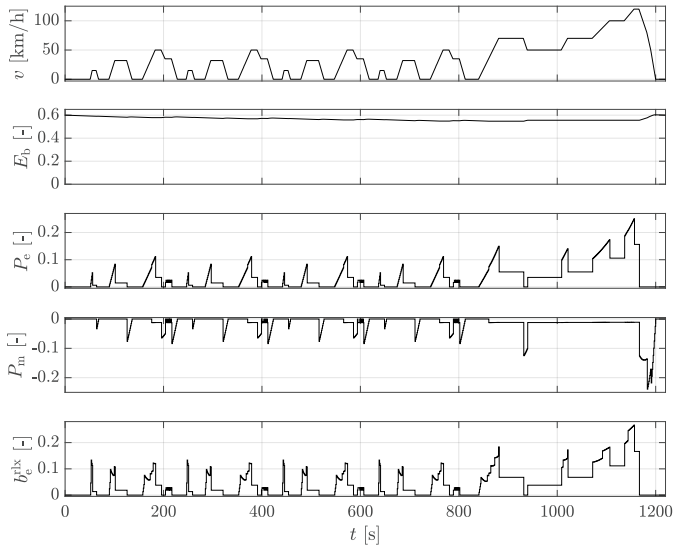

Fig. 7. Results from the relaxed LP for the NEDC.

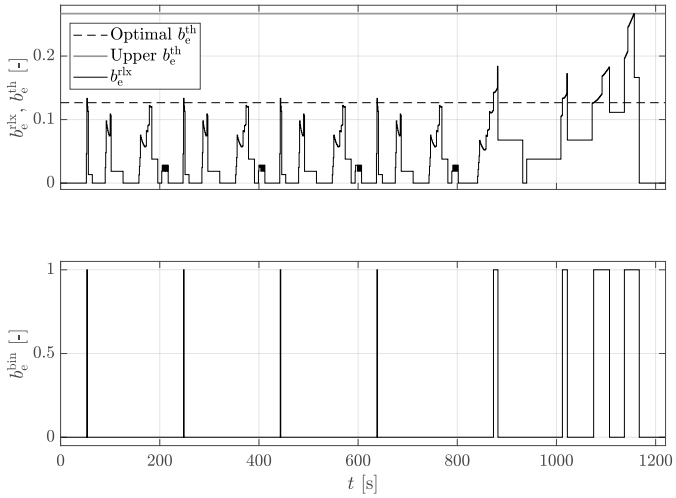

Fig. 8. Simulation results after the second step of the algorithm. In the first plot the relaxed variable $b_{\mathrm{e}}^{\mathrm{rlx}}$ and the upper (gray line) and optimal (black dashed line) thresholds $b_{\mathrm{e}}^{\mathrm{th}}$ are indicated. The second plot represents the resulting optimal on/off engine strategy.

Fig. 7 shows the results obtained in the first step of the algorithm using the New European Driving Cycle (NEDC). The variation of E_{b} is marginal since the engine is operated at the maximum efficiency of the non-relaxed Willans approximation, making load point shifting not profitable. The bottom plot in Fig. 7 shows the optimization variable $b_{\mathrm{e}}^{\mathrm{rlx}}$, highlighting where the engine is turned on and how much of the maximum fuel power is requested.

3.2 TPBVP

We devise a bisection algorithm that takes as an input $b_{\mathrm{e}}^{\mathrm{rlx}}$ and converts it to a binary signal. Since the higher is $b_{\mathrm{e}}^{\mathrm{rlx}}$, the higher is P_{e} in the non-relaxed Willans approximation and, thus, the more efficient is the engine, we turn on the engine where it has the largest efficiency selecting its on/off policy as

$$b_{\mathrm{e}}^{\mathrm{bin}} = \begin{cases} 1 & \text{if } b_{\mathrm{e}}^{\mathrm{rlx}} \geq b_{\mathrm{e}}^{\mathrm{th}} \\ 0 & \text{if } b_{\mathrm{e}}^{\mathrm{rlx}} < b_{\mathrm{e}}^{\mathrm{th}} \end{cases} , \tag{33}$$

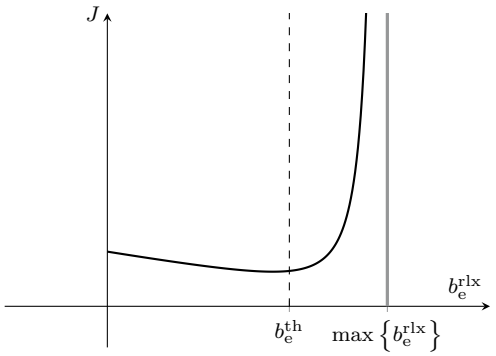

Fig. 9. Objective function J in the bisection algorithm.

where the constant threshold $b_{\mathrm{e}}^{\mathrm{th}} \in [0, 1]$ is subject to identification. This procedure is shown in Fig. 8. Specifically, we want to find the largest $b_{\mathrm{e}}^{\mathrm{th}}$ for which

$$b_{\mathrm{e}} = b_{\mathrm{e}}^{\mathrm{bin}} \tag{34}$$

would still result in a feasible problem (21). Therefore, we devise a bisection algorithm to find $b_{\mathrm{e}}^{\mathrm{bin}}$. Specifically, we first extend Problem (21) by introducing a slack variable defined as

$$\varepsilon = \max\{0, P_{\mathrm{req}} - P_{\mathrm{p,fd}}\} , \tag{35}$$

to measure the problem infeasibility. The objective function is

$$J := \int_{t_0}^{t_{\mathrm{f}}} \Big(P_{\mathrm{f}}(t) + k_{\varepsilon} \cdot \varepsilon(t) \Big) \, \mathrm{d}t \tag{36}$$

and the optimization problem is relaxed to the TPBVP

$$\begin{aligned} &\min \quad J \\ &\text{s.t. } (2), (3), (5), (7), (8), (10), (11), (13), \\ &\quad (14), (16), (19), (34), (35) \\ &\quad E_{\mathrm{b}}(t_0) = E_{\mathrm{b,i}} \\ &\quad E_{\mathrm{b}}(t_{\mathrm{f}}) = E_{\mathrm{b,f}} \ , \end{aligned} \tag{37}$$

which can be parsed to a LP and where k_{ε} is a large positive coefficient to penalize infeasibility.

Fig. 9 shows a qualitative sketch highlighting how the objective (36) varies as a function of the threshold $b_{\mathrm{e}}^{\mathrm{th}}$. The bisection algorithm is detailed in Algorithm 1. It terminates when the tolerance $\Delta b_{\mathrm{e}}^{\mathrm{tol}}$ is met after $\log_2(\max\{b_{\mathrm{e}}^{\mathrm{rlx}}(t)\}/\Delta b_{\mathrm{e}}^{\mathrm{tol}})$ iterations.

3.3 MPBVP

After solving the TPBVP detailed in Section 3.2 for the complete driving cycle, i.e., $t_0 = 0$, $t_{\mathrm{f}} = T$, $E_{\mathrm{b,i}} = E_{\mathrm{b},0}$ and $E_{\mathrm{b,f}} = E_{\mathrm{b,target}}$, we check the path constraint $E_{\mathrm{b}}^{\star}(t) \geq E_{\mathrm{b,min}}$.
If this condition is satisfied, we return the optimal solution of the TPBVP, otherwise we use Algorithm 2 inspired by [Rousseau et al., 2007], and theoretically proven in [van Keulen et al., 2014], to deal with path constraints. The main rationale is to split the problem into sub-problems between the constraint violation points and solve them one by one, until each becomes feasible.

4. RESULTS

This section presents the results obtained by implementing the developed TB-LP algorithm on the NEDC. We compare them to the globally optimal solution obtained by solving the MILP parsed in Section 2.3. All computations are conducted on a Dell XPS15 Desktop PC with an

Algorithm 1. TPBVP algorithm

Solve Problem (32) and get $b_{\mathrm{e}}^{\mathrm{rlx}}$
$b_{\mathrm{e}}^{\mathrm{th,l}} = 0$
$b_{\mathrm{e}}^{\mathrm{th,r}} = \max\left\{b_{\mathrm{e}}^{\mathrm{rlx}}(t)\right\}$
while $b_{\mathrm{e}}^{\mathrm{th,r}} - b_{\mathrm{e}}^{\mathrm{th,l}} > \Delta b_{\mathrm{e}}^{\mathrm{tol}}/2$ **do**
  $b_{\mathrm{e}}^{\mathrm{th}} = \left(b_{\mathrm{e}}^{\mathrm{th,l}} + b_{\mathrm{e}}^{\mathrm{th,r}}\right)/2$
  $b_{\mathrm{e}}^{\mathrm{bin}} = \left(b_{\mathrm{e}}^{\mathrm{rlx}} \geq b_{\mathrm{e}}^{\mathrm{th}}\right)$
  Solve Problem (37) and get $\varepsilon(t)$
  if $\int_{t_0}^{t_{\mathrm{f}}} \varepsilon(t)\,\mathrm{d}t > 0$ **then**
    Problem infeasible
    $b_{\mathrm{e}}^{\mathrm{th,r}} = b_{\mathrm{e}}^{\mathrm{th}}$
  else
    Problem feasible
    $b_{\mathrm{e}}^{\mathrm{th,l}} = b_{\mathrm{e}}^{\mathrm{th}}$
  end
end
$b_{\mathrm{e}}^{\mathrm{bin}} = \left(b_{\mathrm{e}}^{\mathrm{rlx}} \geq b_{\mathrm{e}}^{\mathrm{th,l}}\right)$
Solve feasible Problem (37) and get $E_{\mathrm{b}}^{\star}(t)$ and $P_{\mathrm{m}}^{\star}(t)$
$b_{\mathrm{e}}^{\star}(t) = b_{\mathrm{e}}^{\mathrm{bin}}(t)$
return $x^{\star}(t) = E_{\mathrm{b}}^{\star}(t)$ and $u^{\star}(t) = \left(P_{\mathrm{m}}^{\star}(t), b_{\mathrm{e}}^{\star}(t)\right)$

Algorithm 2. MPBVP algorithm

$t_0 = 0$
$t_{\mathrm{f}} = T$
$E_{\mathrm{b,i}} = E_{\mathrm{b},0}$
$E_{\mathrm{b,f}} = E_{\mathrm{b,target}}$
while $t_0 \neq T$ **do**
  $[x^{\star}(t), u^{\star}(t)] = \mathrm{TPBVP}_{\mathrm{algorithm}}(t_0, t_{\mathrm{f}}, E_{\mathrm{b}}(t_0), E_{\mathrm{b}}(t_{\mathrm{f}}))$
  if $E_{\mathrm{b}}(t) < E_{\mathrm{b,min}}$ **then**
    $t_{\mathrm{f}} = \arg\min_{t\in[t_0,t_{\mathrm{f}}]} E_{\mathrm{b}}(t)$
    $E_{\mathrm{b,f}} = E_{\mathrm{b,min}}$
  else
    $t_0 = t_{\mathrm{f}},\ t_{\mathrm{f}} = T,\ E_{\mathrm{b,i}} = E_{\mathrm{b,min}},\ E_{\mathrm{b,f}} = E_{\mathrm{b,target}}$
    append $x^{\star}(t), u^{\star}(t)$ to $\mathbf{x}^{\star}(t), \mathbf{u}^{\star}(t)$
  end
end
return $\mathbf{x}^{\star}(t)$ and $\mathbf{u}^{\star}(t)$

Intel Core i7-6700HQ CPU and 16 GB RAM running Ubuntu 16.04. To parse the LP and the MILP we used YALMIP [Löfberg, 2004], and the adopted convex solver is CPLEX. First, we assess the performance of our algorithm by considering different lower bounds $E_{\mathrm{b,min}}$ under the charge-sustaining constraint $E_{\mathrm{b,target}} = E_{\mathrm{b},0}$. Second, we perform a parametric study to compute the achievable fuel consumption for different battery targets.

4.1 Solution for Different Path Constraints

We set the lower bound on $E_{\mathrm{b,min}}$ to zero. Fig. 10 shows that the solution provided by the proposed TB-LP algorithm is close to the one obtained by solving the MILP. The lower bound on the path constraint is not active (i.e., the condition $E_{\mathrm{b}}^{\star}(t) \geq E_{\mathrm{b,min}}$ is always satisfied), thus the algorithm terminates after just one iteration of the TPBVP branch, returning a constant value of $b_{\mathrm{e}}^{\mathrm{th}}$. Table 1 collects and compares the results, highlighting a slightly higher fuel consumption for the TB-LP algorithm, whilst showing a significant reduction of the computational time.

Fig. 11 presents the results when the lower bound on the normalized battery energy is set equal to 0.4. The lower

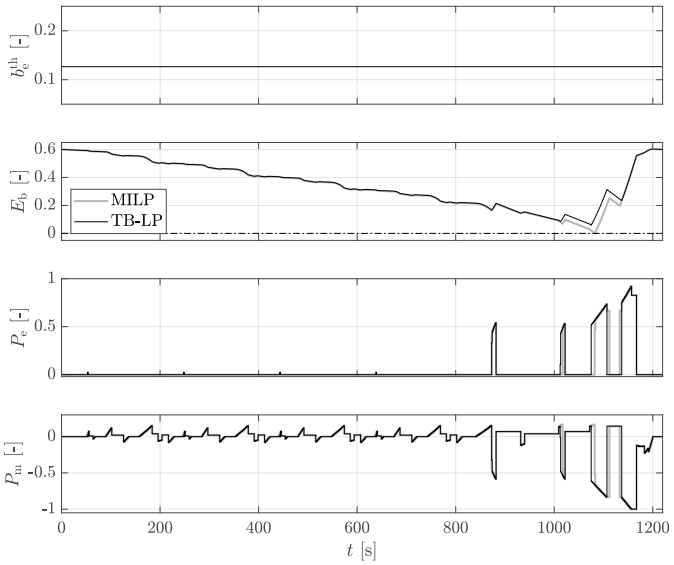

Fig. 10. NEDC, $E_{\mathrm{b,min}} = 0$ (dash-dotted line).

	MILP	TB-LP
Computational time [s]	430.89	6.49
Fuel consumption difference [%]	–	+0.23

Table 1. Comparison for $E_{\mathrm{b,min}} = 0$.

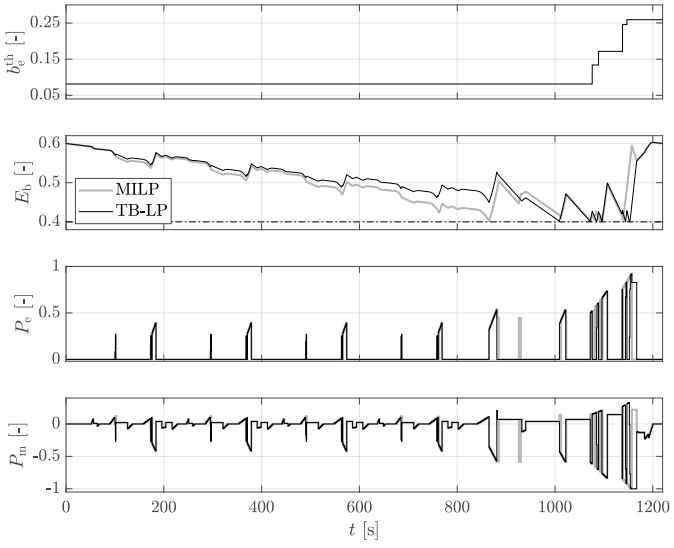

Fig. 11. Results on the NEDC with $E_{\mathrm{b,min}} = 0.4$ (dash-dotted line).

	MILP	TB-LP
Computational time [s]	3237.80	53.95
Fuel consumption difference [%]	–	+0.33

Table 2. Comparison for $E_{\mathrm{b,min}} = 0.4$.

path constraint is active and the MPBVP algorithm iterates five times to reach convergence, returning a piecewise constant value of $b_{\mathrm{e}}^{\mathrm{th}}$. In terms of fuel consumption, the solutions provided by the MILP and the TB-LP are very close, with a difference of just +0.33% as pointed out in Table 2. Also in this case the computational time is reduced by two orders of magnitude.

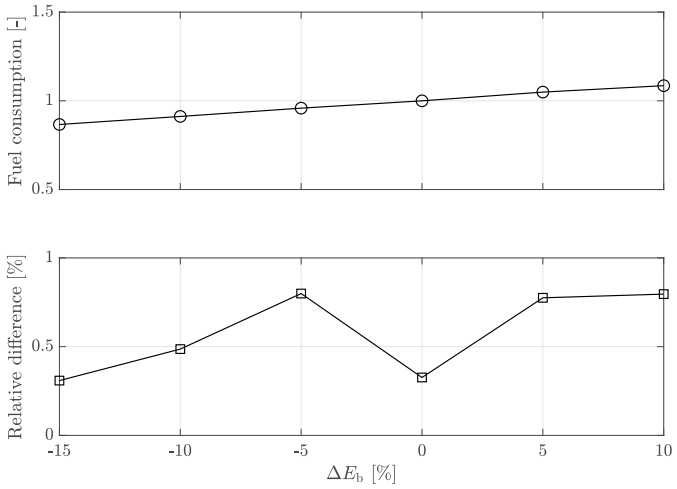

Fig. 12. Scan on different E_b targets. The first plot represents the impact on total fuel consumption (normalized w.r.t. $\Delta E_b = 0$). The second plot shows the difference in fuel consumption compared to the MILP.

4.2 Scan on Battery Targets

To showcase the effectiveness of the proposed algorithm we also provide a parameter study on the impact of different $E_{b,target}$ on the achievable fuel consumption. The complete computation took 297 s. Fig. 12 shows a linear relationship between fuel and battery usage as well as good coherence with the MILP results.

5. CONCLUSION

This paper presented an optimization algorithm to quickly assess the minimum-fuel engine on/off control for the energy management of a hybrid electric vehicle. After identifying a piecewise affine model of the powertrain, we parsed the fuel-optimal control problem to a mixed-integer linear program (MILP) with a binary variable representing the engine on/off signal. Finally, we devised an iterative algorithm to rapidly solve the multi-points boundary value problem arising from the battery size constraints as a sequence of two-points boundary value problems, each tackled as a sequence of linear programs iterating on the engine on/off variable. We tested our approach on the New European Driving Cycle and the results showed good coherence with the globally optimal MILP solution, whilst achieving significantly lower computational times by roughly two orders of magnitude. To demonstrate the effectiveness of the proposed algorithm, we then investigated the impact of different battery targets on the achievable fuel consumption.

Future research could extend the presented algorithm to account for scenarios where the upper battery energy limit constraint is active and assess the optimal gear-shift strategy. Furthermore, this approach could be extended to topology optimization and real-time control.

ACKNOWLEDGEMENTS

We are very thankful to Mr. Nicolas Lanzetti for helping us generating the schematic representations. Moreover, we express our gratitude to Dr. Ilse New for proofreading this paper.

REFERENCES

Soren Ebbesen, Mauro Salazar, Philipp Elbert, Carlo Bussi, and Christopher H. Onder. Time-optimal control strategies for a hybrid electric race car. *IEEE Transactions on Control Systems Technology*, 26(1):233–247, 2018.

Philipp Elbert, Soren Ebbesen, and Lino Guzzella. Implementation of dynamic programming for n-dimensional optimal control problems with final state constraints. *IEEE Transactions on Control Systems Technology*, 21 (3):924–931, 2013.

Lino Guzzella and Christopher H. Onder. *Introduction to modeling and control of internal combustion engine systems*. Springer, Berlin, 2 edition, 2010.

Lino Guzzella and Antonio Sciarretta. *Vehicle propulsion systems*. Springer, Berlin, 3 edition, 2013.

Theo Hofman, Maarten Steinbuch, Roell Van Druten, and Alex Serrarens. Rule-based energy management strategies for hybrid vehicles. *International Journal of Electric and Hybrid Vehicles*, 1(1):71–94, 2007.

Lars Johannesson, Nikolce Murgovski, Erik Jonasson, Jonas Hellgren, and Bo Egardt. Predictive energy management of hybrid long-haul trucks. *Control Engineering Practice*, 41:83–97, 2015.

Johan Löfberg. Yalmip : A toolbox for modeling and optimization in MATLAB. In *Proceedings of the CACSD Conference*, Taipei, Taiwan, 2004. URL `http://users.isy.liu.se/johanl/yalmip`.

Nikolce Murgovski, Lars Johannesson, Xiaosong Hu, Bo Egardt, and Jonas Sjoberg. Convex relaxations in the optimal control of electrified vehicles. In *American Control Conference (ACC), 2015*, pages 2292–2298. IEEE, 2015.

Tobias Nüesch, Alberto Cerofolini, Giorgio Mancini, Nicolò Cavina, Christopher Onder, and Lino Guzzella. Equivalent consumption minimization strategy for the control of real driving nox emissions of a diesel hybrid electric vehicle. *Energies*, 7(5):3148–3178, 2014a.

Tobias Nüesch, Philipp Elbert, Michael Flankl, Christopher Onder, and Lino Guzzella. Convex optimization for the energy management of hybrid electric vehicles considering engine start and gearshift costs. *Energies*, 7 (2):834–856, 2014b.

Arthur Richards and Jonathan How. Mixed-integer programming for control. In *American Control Conference, 2005. Proceedings of the 2005*, pages 2676–2683. IEEE, 2005.

Gregory Rousseau, Delphine Sinoquet, and Pierre Rouchon. Constrained optimization of energy management for a mild-hybrid vehicle. *Oil Gas Sci. Technol. - Rev. IFP Energies nouvelles*, 62(4):623–634, 2007.

Mauro Salazar, Camillo Balerna, Philipp Elbert, Fernando P. Grando, and Christopher H. Onder. Real-time control algorithms for a hybrid electric race car using a two-level model predictive control scheme. *IEEE Transactions on Vehicular Technology*, 66(12):10911–10922, 2017a.

Mauro Salazar, Philipp Elbert, Soren Ebbesen, Carlo Bussi, and Christopher H. Onder. Time-optimal control policy for a hybrid electric race car. *IEEE Transactions on Control Systems Technology*, 25(6):1921–1934, 2017b.

Mauro Salazar, Camillo Balerna, Eugenio Chisari, Carlo Bussi, and Christopher H. Onder. Equivalent lap time minimization strategies for a hybrid electric race car. *accepted for IEEE Control and Decision Conference*, 2018.

Thijs van Keulen, Jan Gillot, Bram de Jager, and Maarten Steinbuch. Solution for state constrained optimal control problems applied to power split control for hybrid vehicles. *Automatica*, 50(1):187–192, 2014.